SLAC-PUB-14156

Transmission and Radiation of an Accelerating Mode in a Photonic Bandgap Fiber

C.-K. Ng, R. J. England, L.-Q. Lee, R. Noble, V. Rawat and J. Spencer
SLAC National Accelerator Laboratory
2575 Sand Hill Road, Menlo Park, CA 94025, USA

Abstract

A hollow core photonic bandgap (PBG) lattice in a dielectric fiber can provide high gradient acceleration in the optical regime, where the accelerating mode resulting from a defect in the PBG fiber can be excited by high-power lasers. Efficient methods of coupling laser power into the PBG fiber are an area of active research. In this paper, we develop a simulation method using the parallel finite-element electromagnetic suite ACE3P to study the propagation of the accelerating mode in the PBG fiber and determine the radiation pattern into free space at the end of the PBG fiber. The far-field radiation will be calculated and the mechanism of coupling power from an experimental laser setup will be discussed.

1 Introduction

The photonic bandgap fiber proposed by Lin [1] has shown through simulation the possibility of confining an accelerating mode in an energy band gap existing in a periodic lattice of vacuum holes with a defect located in the center. Such fibers can in principle achieve high gradients when operated in the optical regime using lasers for excitation of the accelerating mode. However, the mechanism of coupling power into the PBG fiber has not been addressed. Conventional microwave accelerating structures use metallic waveguides for coupling power from external power sources. In the microwave regime, an accelerating structure is normally connected to beampipes at both ends so that the accelerating mode is confined in the structure for a standing wave or propagates in the forward direction for a traveling wave. In the optical to infrared regime, the power cannot be delivered through a metallic waveguide for distances L $\gg$ 200 wavelengths because of the large wall loss at high frequencies, and thus an optical fiber waveguide should be considered. It is also important that the power coupling into the PBG fiber will propagate in the forward direction along the beam direction using the traveling, defect mode for acceleration. In order to understand the complexities involved in designing a coupler for the PBG fiber, it is instructive to study both the transmission and radiation pattern from the propagation of the accelerating mode in the PBG fiber through numerical simulation, which will provide insights for the mechanism of exciting the

Work supported in part by US Department of Energy contract DE-AC02-76SF00515.

accelerating mode in an experimental setup. The details of coupler designs using optical fiber waveguides will be reported in a subsequent paper [3].

This work will focus on numerical simulations of the propagation of the defect mode in the PBG fiber and from the fiber into free space. We use the electromagnetic simulation package ACE3P [2] developed at SLAC for the simulations. ACE3P is a suite of parallel electromagnetic codes based on the finite-element method, and it consists of solvers in both the frequency and time domains. There are several advantages of using these codes for our simulations. First, tetrahedral finite elements with quadratic curved surfaces are well suited for modeling the curved geometries of the PBG fiber with high fidelity. The finite elements also have higher-order basis function representations which allow solutions with high accuracy. Second, the simulation of the propagation of the accelerating mode requires its excitation at a port boundary of the computational volume. The electromagnetic field pattern of the defect mode can be solved by the frequency-domain eigensolver Omega3P [4] in ACE3P, and then loaded into the time-domain solver T3P [5], where appropriate boundary conditions can be imposed on the outer surfaces of the computational volume to terminate the propagation of electromagnetic waves. Third, the parallel capability of these codes allows large problems to be solved on parallel computers. This is useful for simulating the radiation into free space from the accelerating mode by using a large computational volume.

This paper is organized as follows. In section 2, we use the frequency-domain eigensolver Omega3P to determine the defect mode in the PBG fiber. In section 3, we describe a numerical procedure to simulate the propagation of the defect mode traveling in the PBG fiber using the time-domain code T3P. In section 4, we calculate the power radiated from the accelerating mode into free space and determine the far-field radiation pattern. A summary of the results is given in the last section.

2 Defect Mode in Photonic Bandgap Fiber

The PBG fiber (see Fig. 1) proposed by Lin consists of circular holes in a lattice with spacing a between the centers of neighboring holes, and hence the resulting lattice has a 6-fold symmetry. The holes have a radius of $0.35a$. In order to introduce a defect in the lattice, one hole is replaced by another with a radius of $0.52a$. The material of the fiber has a dielectric constant of 2.13. In Lin's paper, the defect mode is obtained using the Plane Wave Method [6] with the propagation constant $\beta = k_z/k_0 = 1$, where k_0 and k_z are the wave number and its component along the propagation z-axis, respectively. Here we used Omega3P, a Maxwell eigensolver that was developed to solve for the resonant modes of an accelerator cavity. The simulation uses a thin slab of the PBG fiber with circular cross section, which is truncated at five lattice constants from the center of the defect. By imposing different boundaries conditions at opposite sides of the slab, the frequencies of standing wave modes are obtained with their wavelengths determined by the slab thickness. Omega3P solves for a number of modes above a certain specified frequency, and the defect mode can be identified from the field patterns of these modes. By repeating the simulation for different slab thickness, the frequency of the defect mode as a function of the propagation constant is obtained.

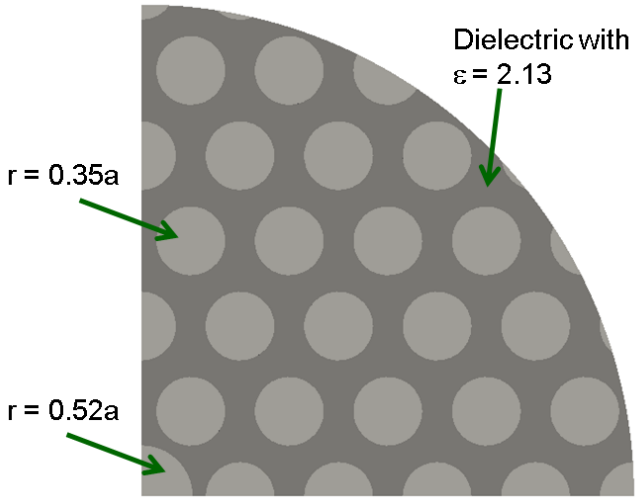

Figure 1: One quarter of the Lin PBG structure where a defect hole is located at the center in a lattice consisting of regularly spaced holes of the same size.

The dispersion curve is shown in Fig. 2, from which the frequency of the synchronous mode propagating at the speed of light is found to be $8.2c/a$, the same as that obtained in Ref. [1].

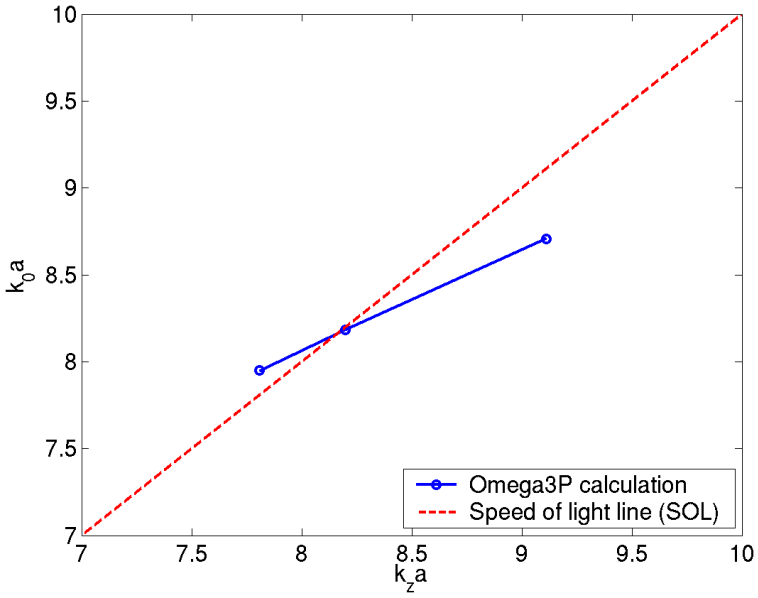

Figure 2: Dispersion curve calculated by Omega3P near the PBG defect mode.

The longitudinal and transverse electric field patterns, and the transverse magnetic field pattern are shown in Fig. 3. All relevant figures in this paper use a rainbow color scheme to represent magnitude with the red and blue being the maximum and minimum, respectively. It can be seen that the defect mode is TM-like with a uniform distribution of longitudinal field inside the defect hole that can be used for acceleration. All the field components exhibit the six-fold symmetry of the lattice, with their maxima located at a distance 1-1.5 a from the center of the defect. The values of the transverse electric and magnetic fields at different locations of the cross section of the PBG

fiber obtained from Omega3P are written to files which will then be read in as inputs to the time domain solver T3P for studying mode propagation. It is instructive to see how the defect mode is confined by studying the decay of its electromagnetic fields from the center of the defect hole. Fig. 4 shows the variations of the longitudinal component of the electric field as a function of the transverse position (in units of a) along the x-axis and y-axis. The field decays to very small value (less than several $\%$ of the maximum) when the distance is bigger than $4a$ in both directions. In the defect hole, the field remains essentially constant. This is in good agreement with the results obtained in Ref. [1].

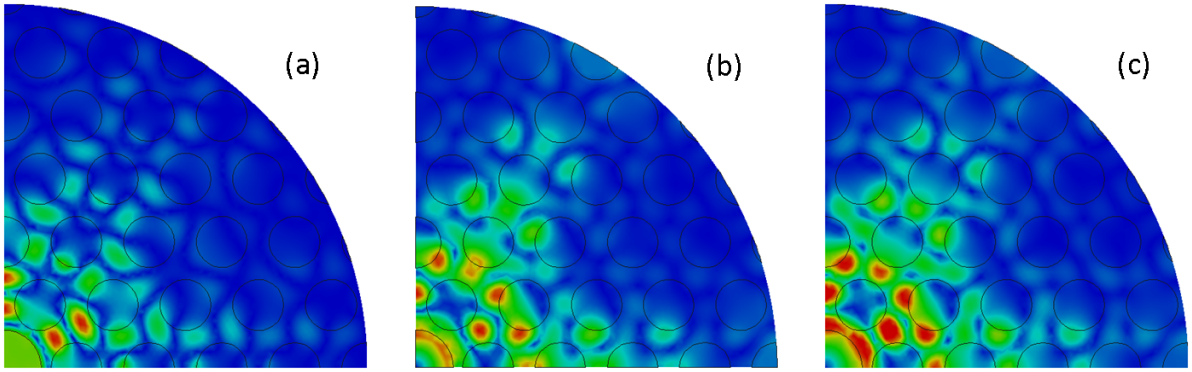

Figure 3: Defect mode in the PBG fiber: (a) longitudinal electric field; (b) transverse electric field; (c) transverse magnetic field.

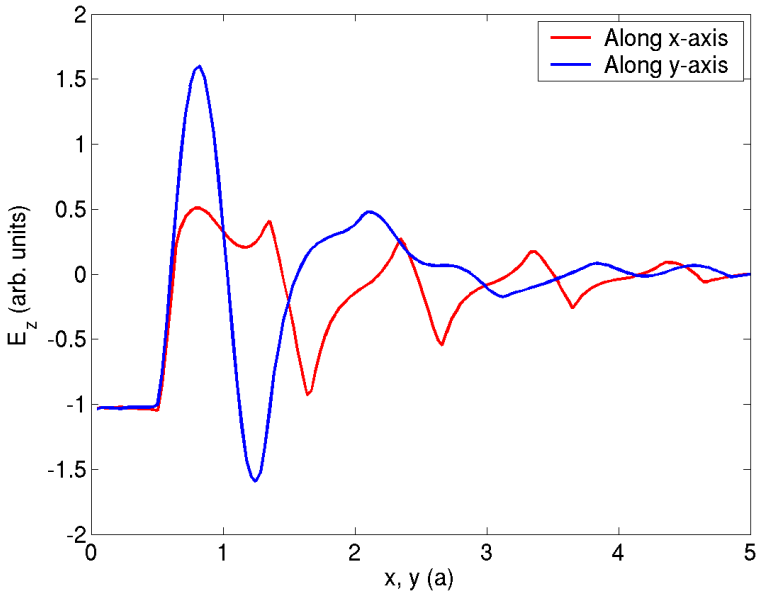

Figure 4: Variations of the longitudinal electric field of the defect mode along the x-axis and y-axis.

3 Propagation of Defect Mode

We use the time domain code T3P to study the propagation of the defect mode in the PBG fiber. Consider a slab of the PBG fiber with more than 2λ thickness as shown in Fig. 5, where λ is the wavelength of the source. The ends of the slab are treated as waveguide ports such that the defect mode propagates from the input port on the left, transits through the slab, and exits at the output port on the right. The transverse components of the electric and magnetic fields for the defect mode obtained using Omega3P in the previous section are loaded at the input port as an external excitation in T3P. In order to minimize excitations of frequency contents other than the defect mode frequency, a narrowband pulse with a slow rise time is driven at the input port. Typically, a rise time of 20-30 periods is sufficient to maintain the monochromatic feature of the excitation. Absorbing boundary conditions [5] are imposed at both the input and output ports to terminate any electromagnetic field propagation so that reflection back to the computational volume is minimized. The time domain simulation is carried out until steady state is reached. Fig. 5(a) and (b) show the electric field pattern during the rise time of the driven pulse and that at steady state, respectively. It can be seen that the steady state field demonstrates the establishment of a traveling mode in the PBG fiber.

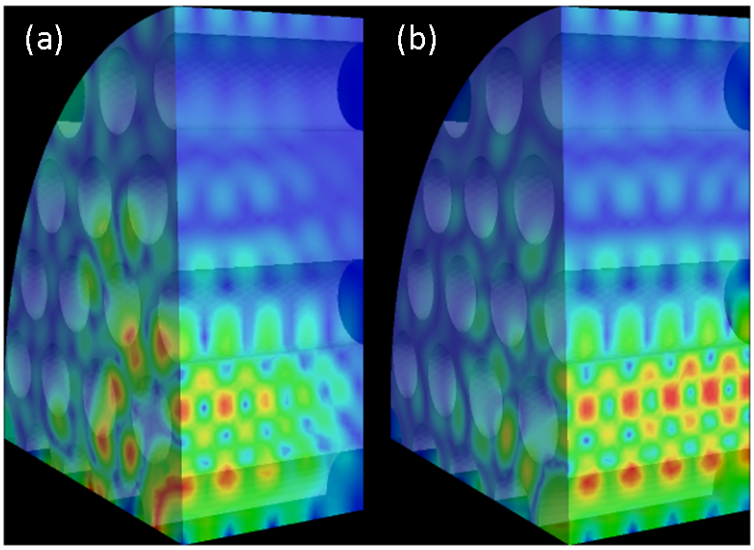

Figure 5: Snapshots of electric field amplitude for propagation of defect mode in fiber slab: (a) during transient; (b) at steady state.

The instantaneous power at the input and output ports is determined by integrating the Poynting flux over the areas of the ports. Fig. 6 shows the power as a function of time at these ports. The positive and negative values of the power indicate that the net power flow is outward and inward at the port, respectively. At the input port, the evolution of the power follows that of the driven pulse and the power propagates in the forward direction into the PBG fiber slab. The power at the output end has a similar pattern as that at the input port, and its magnitude is the same (with less than 1% difference) but of opposite sign as that of the excitation at the input port, indicating that

the power flows out from the PBG fiber. There is a time delay between the input and output signals determined by the group velocity of the traveling wave, which is found to be $0.61c$, in agreement with that obtained in Ref. [1].

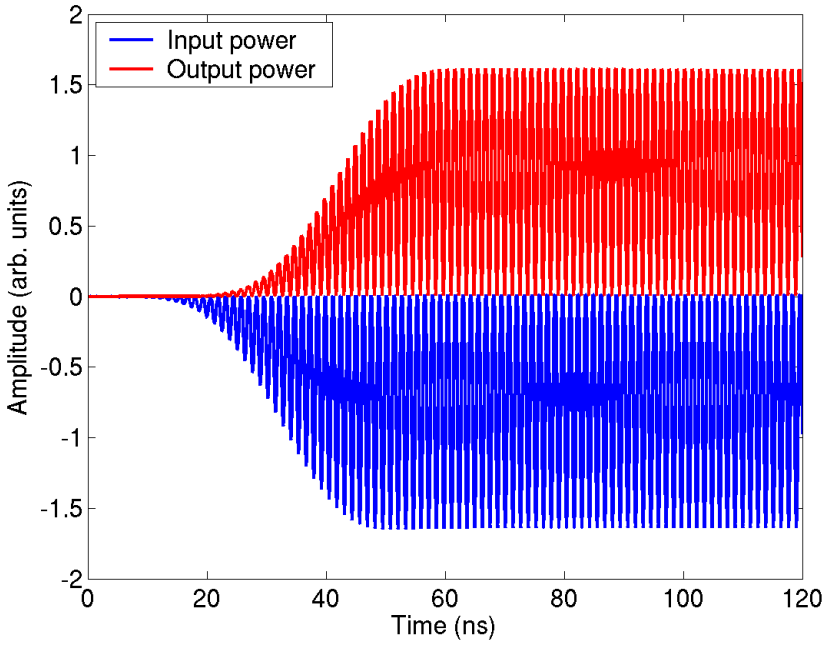

Figure 6: Power transmission in the PBG fiber slab. The blue and red curves represent the input and output pulse, respectively.

4 Simulation of Radiation from Defect Mode

4.1 Radiation from Defect Mode

To provide insights of how to couple power into the PBG fiber, it is instructive to study the inverse problem first, namely the radiation pattern from the propagation of the defect mode into free space. The radiation pattern will provide guidelines to project laser beams near the end of the PBG fiber to excite the defect mode. To this end, we use the time domain code T3P to simulate the model as shown in Fig. 7. Because of symmetry, only one quarter of the PBG fiber is simulated. In this model, a PBG slab is placed in a spherical volume whose spherical surface is terminated using an absorbing boundary condition so that the outgoing waves diffracted at the interface between the PBG fiber and the vacuum will not be reflected back into the computational volume. In a similar manner as discussed in the previous subsection, the defect mode is excited at the input port located at the left end of the PBG slab, propagates through the slab, and then radiates into free space. Again, to maintain the monochromatic feature of the pulse, a slow rise time is used similar to that in the previous section. In contrast to the previous case of wave propagation in a uniform PBG

slab, the smooth propagation of the electromagnetic fields of the defect mode will be intercepted at the PBG-vacuum interface. Part of the power carried by the defect mode will be reflected and the rest will transmit out the right hand boundary of the PBG and radiate into free space. The radiated electromagnetic waves will be terminated at the surrounding spherical surface for the simulation.

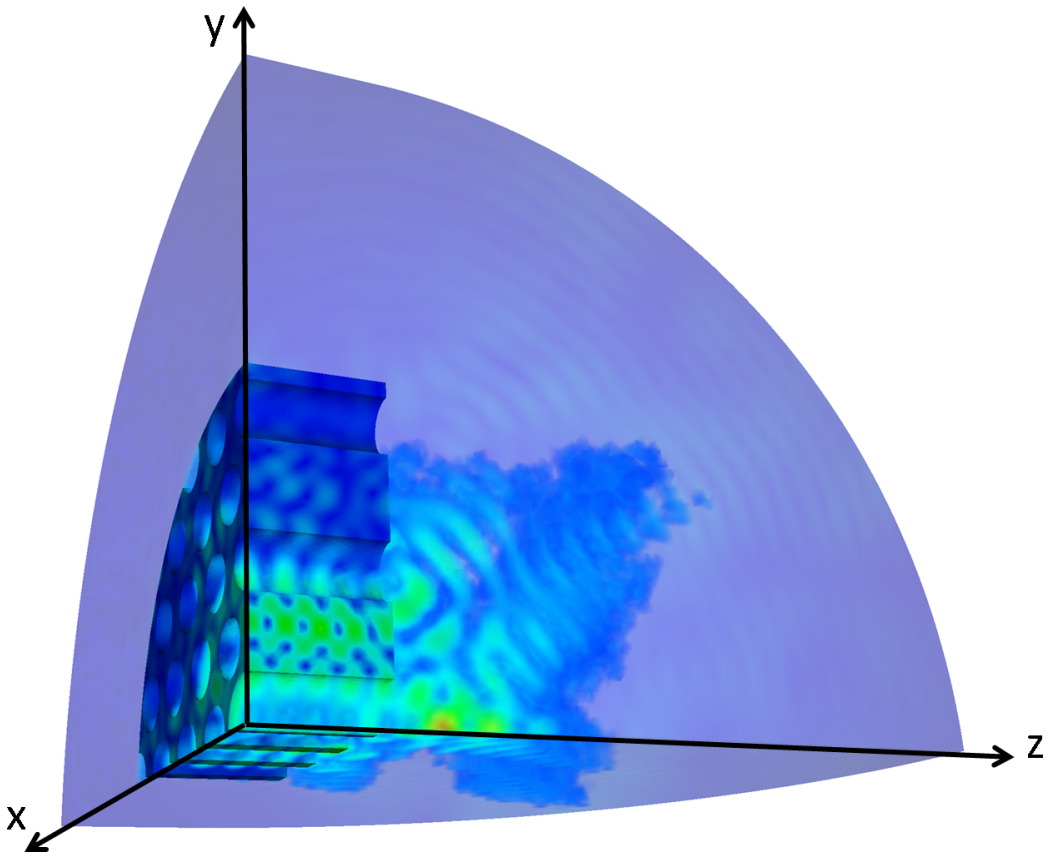

Figure 7: Snapshot of the radiated electric field from the propagation of the defect mode in the fiber. In the simulation, the length of the fiber slab is a little bigger than 2λ and the radius of the sphere enclosing the simulation model is 10λ.

A snapshot of the electric field amplitude at steady state is shown in Fig. 7. It can be seen that the radiated field propagates in a non-uniform manner with power confined in several cones with certain solid angles. The detail of the distribution will be discussed later. The electric field inside the PBG fiber shows the modulation of the forward traveling wave as a result of the reflection at the PBG-vacuum interface. The diffracted wave has an extended high field region shown in red and is located at a distance of about one wavelength in the forward direction along the symmetry axis (z) of the fiber that is due to the constructive interference of the uniform field of the accelerating mode scattering from the exit of the circular defect aperture. The field distributions on the plane perpendicular to the z-axis are shown in Fig. 8 with the electric field still showing strong longitudinal polarization components. Notice that there are other components of the radiation field that are barely visible in Fig. 7 that we will discuss further in Fig. 10.

Fig. 9 shows the power radiated out at the spherical surface of the computational volume, and

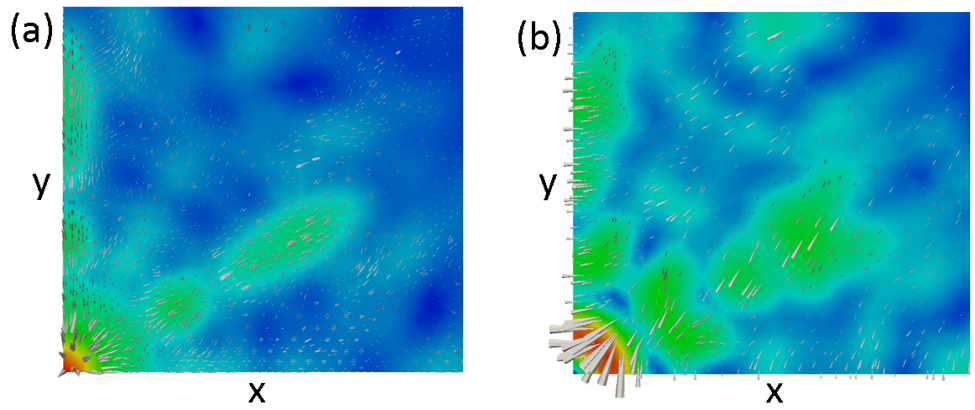

Figure 8: The amplitudes of (a) the electric field and (b) the magnetic field at a distance of about one λ from the PBG-vacuum interface. The cones represent the field vectors and their sizes scale as the magnitudes of the fields.

that reflected back into the PBG fiber. The positive and negative values of the power indicate power flowing outward and inward through a surface, respectively. The time evolution of the instantaneous power at the output spherical surface shows that the electric and magnetic fields of the radiated waves are not in phase, indicating that interference effects from the diffracted waves at this distance are still important to preclude the establishment of a far field radiation pattern. The positive values of the instantaneous power at the input port mean that some power is reflected and propagates backward in the PBG fiber. The averaged radiated and reflected power is found to be about 81% and 19%, respectively.

Fig. 10 shows the radiation pattern on the spherical surface, looking from the longitudinal axis of the PBG fiber. This represents one quarter of the forward hemisphere. Two prominent peaks in the Poynting flux can be seen on the surface. The location of each peak is defined by two angles (θ, ϕ), where θ is the angle between the longitudinal z-axis and the line joining the peak location and the origin defined at the fiber-vacuum interface, and ϕ defined by the projection on the transverse x-y plane of the PBG fiber. Both peaks are located at $\theta = 45^o$ from the longitudinal, symmetry z-axis and the two transverse angles ϕ are at 0^o and 60^o with respect to the x-axis (Fig. 10).

4.2 Far-field Radiation Pattern

Following the procedure in the previous subsection, one can obtain the far-field radiation pattern on the spherical surface by using a forward hemisphere with a large radius $\gg \lambda$. However the computational domain will become very big and the calculation will be very time-consuming. To circumvent this problem, we opt to extract the fields on the plane of the fiber-vacuum interface and use them as excitation sources in calculating the far-field radiation. Fig. 11 shows the electric and magnetic fields on this plane. The field patterns at this plane preserve most of those of the defect mode shown in Fig. 3.

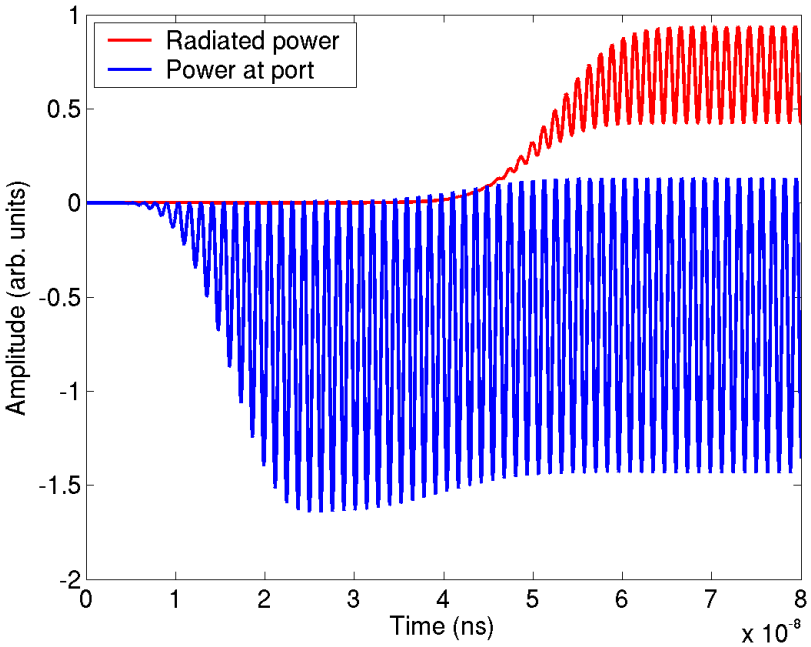

Figure 9: Radiated power (red) and power transmitted at the input port (blue) for the propagation of the defect mode at the end of the fiber.

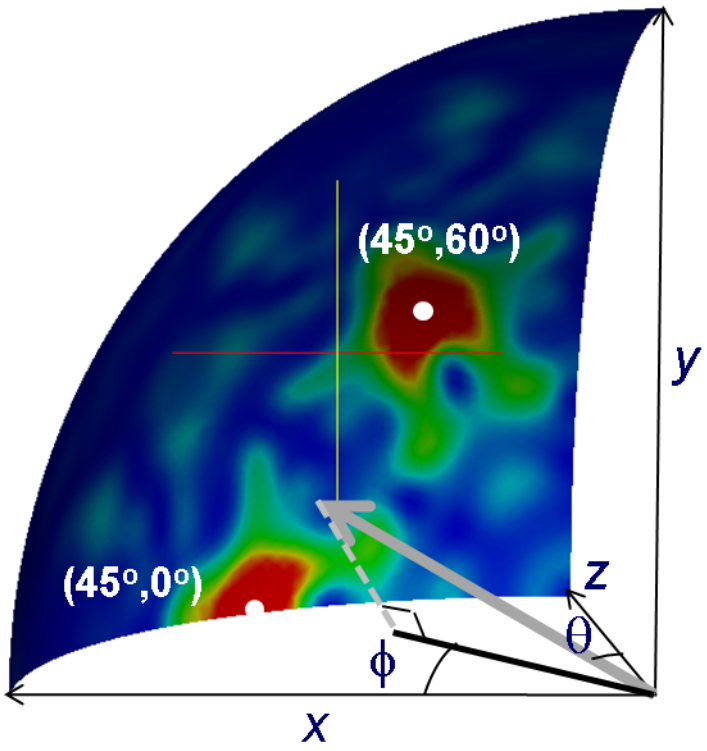

Figure 10: Radiated power pattern in the forward quarter spherical surface (with a radius of $8a$ or about 10λ) from defect mode propagation in the fiber.

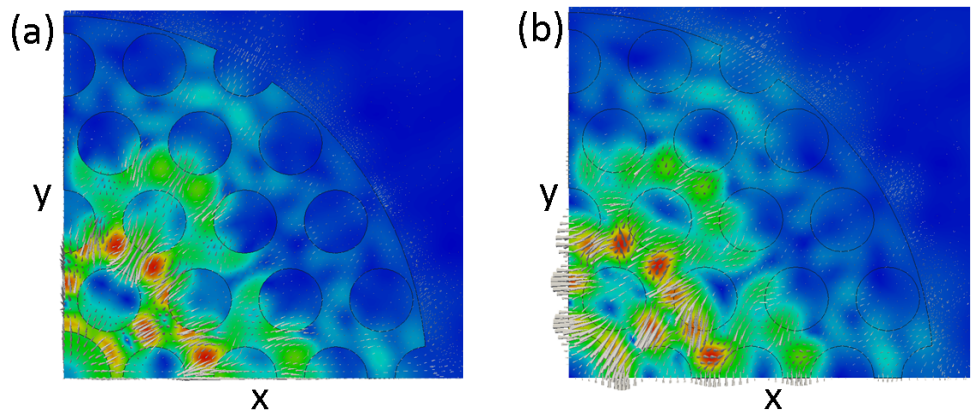

Figure 11: The amplitudes of (a) the electric field and (b) the magnetic field at the PBG-vacuum interface. The cones represent the field vectors and their sizes scale as the magnitudes of the fields.

The far-field radiation is determined using Huygen's Principle [7] and obtained through the following procedure. The source plane is divided into a number of patches using a rectangular grid. Within each grid, the current sources are calculated using the electric and magnetic field vectors obtained from the T3P simulation. Since only a quarter of the structure is simulated in T3P, the source plane representing the full model is obtained by reflecting appropriately the fields through the symmetry planes. The display surface of the far-field radiation is chosen to be a forward hemisphere with its origin at the defect center. The distant spherical surface is also divided into a number of patches, the dimensions of which are set to 0.2λ. The far-field radiation in each patch is determined by all the patches in the source plane through the propagation of the electromagnetic radiation in free space. Thus the computation for the far-field on the whole surface scales as the product of the numbers of the patches in the source plane and radiation surface. A Matlab propagator code [8] was used for the calculation, and the choice of 0.2λ resolution for the surface patches is found to be sufficient to reveal the radiation pattern within a reasonable amount of computational time.

Fig. 12 shows the Poynting flux of the far-field radiation on the hemispherical surface as a function of the radius R of the hemisphere, scaled to the same size for ease of display. The radiation pattern changes drastically from $R = 5\lambda$ to $R = 20\lambda$ and reaches a steady configuration at $R = 80\lambda$. It should be noted that the radiation pattern at 10λ is very similar to that obtained by direct T3P simulation where the radius of the spherical surface enclosing the computation domain is 10λ. Using the source fields determined by a different code [9] for PBG mode calculation and propagating these with the Matlab code shows similar radiation patterns as those shown in Fig. 12, verifying qualitatively the correctness of our calculations. As shown from Fig. 12, the far-field radiation pattern has a six-fold symmetry and is localized in the hot spot regions (indicated by red color) on the downstream surface. Remembering that the z-axis is in the forward direction perpendicular to the source plane, the centers of the hot spots are located at $\theta = 45^o$ from the z-axis, and spaced at 60^o in the azimuth ϕ. This angular dependence agrees well with that obtained from direct simulation using T3P (Fig. 10). To estimate the spatial extent of a hot spot on the

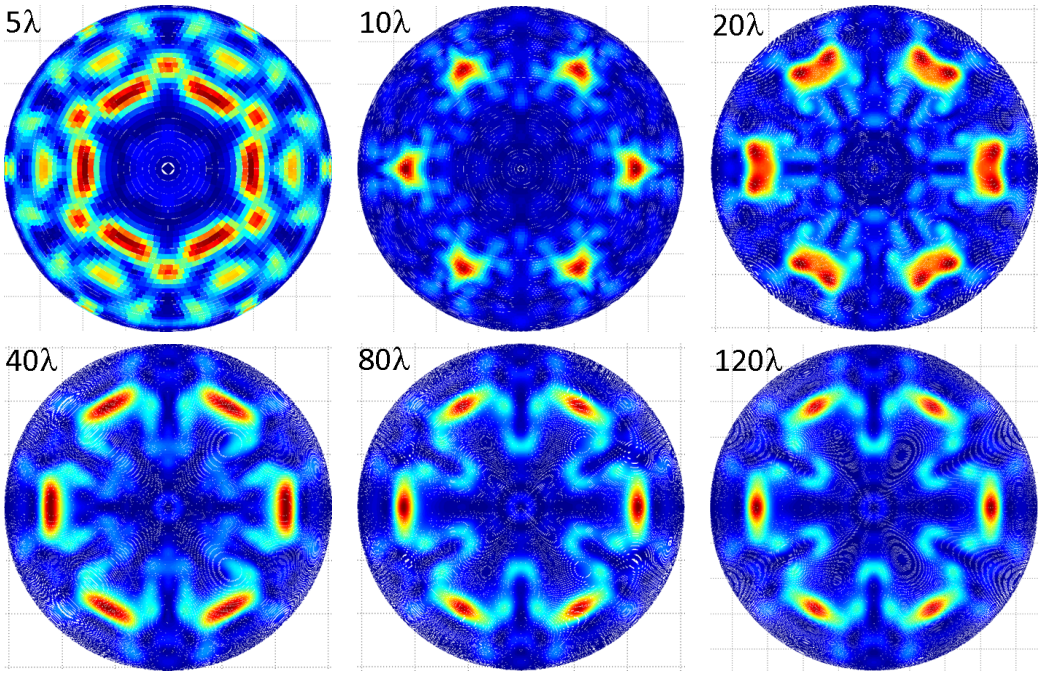

Figure 12: Projection of Poynting flux from the surface of the forward hemisphere onto a circular disk (scaled) as a function of the hemisphere radius at 5λ, 10λ, 20λ, 40λ, 80λ and 120λ.

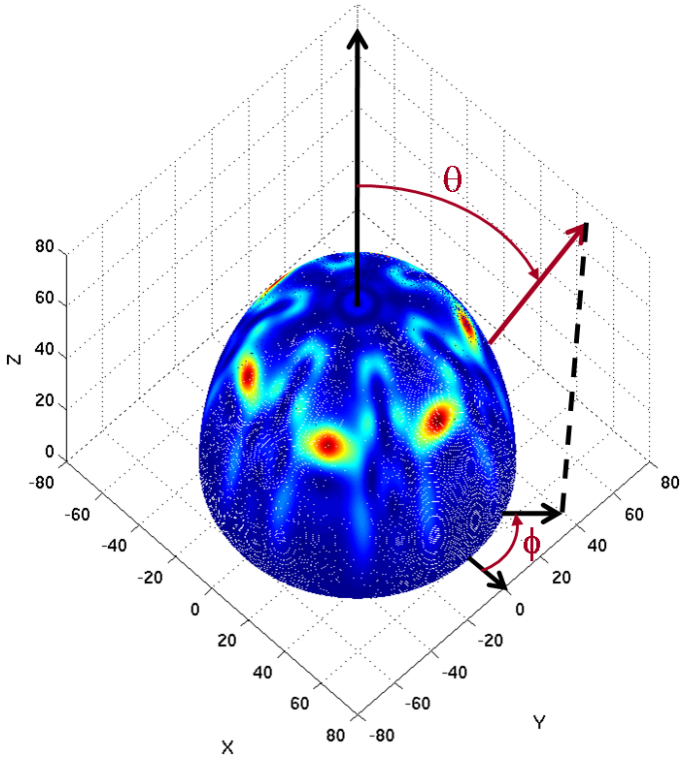

Figure 13: Poynting flux on the surface of the forward hemisphere with radius 80λ. The z-axis is normal to the source plane, and the x- and y-axes define the source plane.

surface as shown in the 3-dimensional plot at $R = 80\lambda$ in Fig. 13, the boundary of the region is defined by the Poynting flux value dropped by two e-foldings of the maximum. It is found that the six hot spots together contain 75% of the radiated power within 33% of the total surface area.

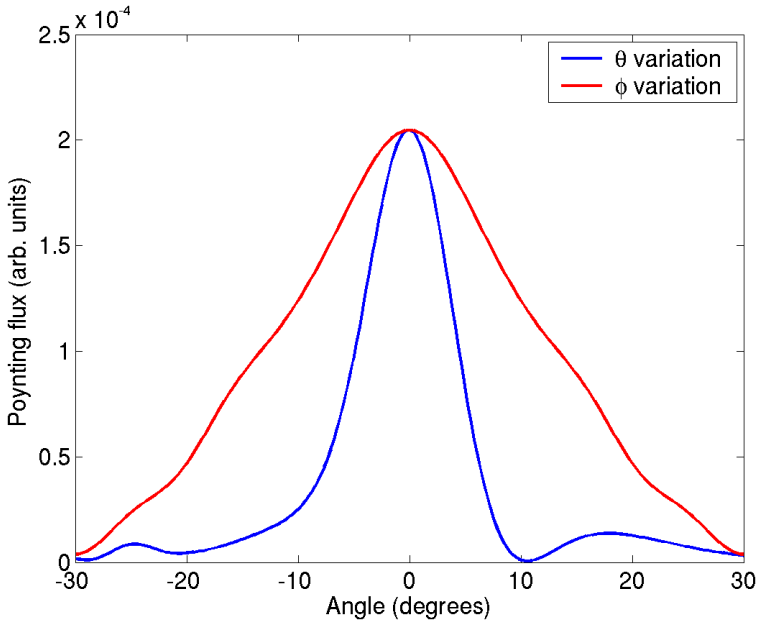

Figure 14: Variations of Poynting flux along the longitude and latitude passing the peak of a hot spot on the forward hemisphere with radius 80λ. The variation along the latitude covers a range of 60^o, the angle of rotation symmetry of the radiation pattern. The variation along the longitude spans from 0-90^o but is predominately confined to about 30^o and is shifted by 45^o so that its peak coincides with that along the latitude for easy comparison.

Figure 14 shows the variations of the Poynting flux along the longitude and latitude passing through the peak of a hot spot on the forward hemisphere with radius 80λ. It can be seen that the shape along the longitude is very close to a Gaussian and the variation along the latitude is rather linear in nature. Figure 15 shows the shape of the hot spot along the longitude and latitude for different hemisphere radii R from 10λ to 120λ. The shape along the longitude is always narrower than that along the latitude. Along the longitude, the width of the Gaussian-like shape gets narrower as R increases until it reaches a steady state above 80λ. Along the latitude, the shape is rather Gaussian-like at $R = 10\lambda$, after which it broadens out with a double-humped profile and changes back to a broad peak with linear drops on both sides when R is greater than 80λ. This illustrates the complicated interference effects contributed by the current sources as one moves away from them. A brief word about radiation and coupling effects in such fiber may be useful here before proceeding because the two are clearly related. For the types of modes of concern here, losses from the sides and ends need to be considered and while these have different fixes, they are both defined by the basic hexagonal symmetry of the lattice. Thus, losses from both sides and ends typically show six-fold symmetry and will be addressed in a subsequent paper where perturbations of the pure hexagonal lattice symmetry about the defect is broken in various periodic and aperiodic

ways.

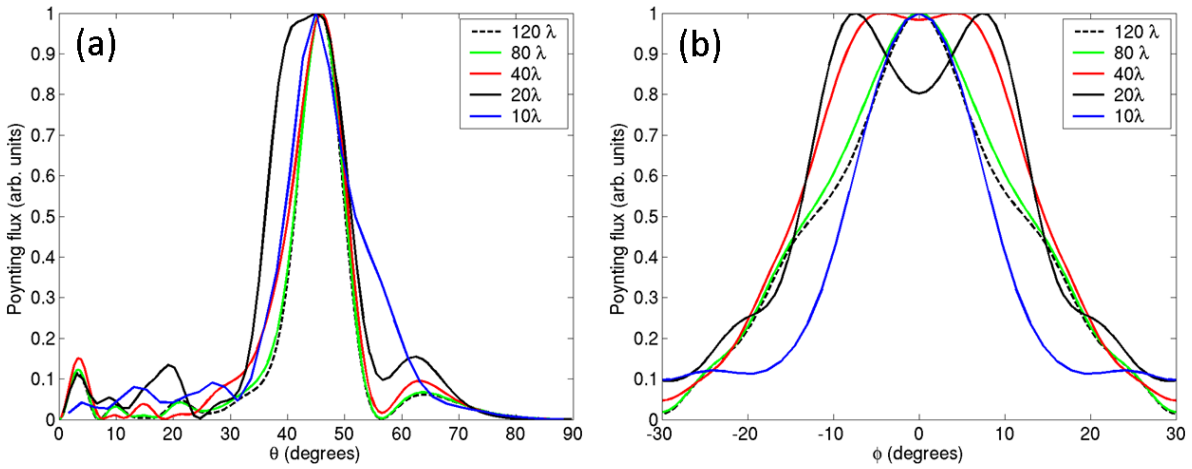

Figure 15: The shapes of a hot spot along (a) the longitude and (b) the latitude for different hemisphere radii (in units of λ).

Fig. 16 shows the polarizations of the electric and magnetic fields at one of the hot spot located in the projected horizontal x-direction. The electric field vectors point towards the pole of the hemisphere along a longitude, and the magnetic field vectors along a latitude on the surface. The polarizations at other hot spots behave in a similar manner by rotating $\phi = 60^o$ with respect to the z-axis. The far-field polarizations are reminiscent of those of the spherical TM_{01} mode, but have strong localized magnitudes in the six hot spots for the PBG fiber, with an $\mathbf{E} \times \mathbf{H}$ structure similar to a laser's TEM beam. Therefore, as a reverse process, six laser beams with their polarizations in phase can be used as a means to direct power from a far distance ($\approx 120\lambda$) to excite the accelerating mode in the PBG fiber.

5 Conclusion

The PBG fiber proposed by Lin [1] has shown through simulation the existence of a defect mode that can be used for particle acceleration. The coupling of power from external power sources has to be efficient in order that the PBG can be a potential candidate for future linear colliders using lasers as excitation sources. We have developed the numerical methods through the parallel electromagnetic finite-element code suite ACE3P to simulate the propagation of the accelerating mode inside the PBG fiber and determine its far-field radiation pattern. The far-field Poynting flux reflects the six-fold symmetry of the geometry of this PBG fiber with the radiated power concentrated in six localized regions. From the polarizations of the radiated fields, the lasers can be aligned in these localized regions to direct power to the PBG fiber to excite the accelerating mode efficiently. This would be the first major step in coupling power to the PBG fiber for the demonstration of laser acceleration. This appears to be a comparatively easy and efficient technique to excite these modes in a way that does not interfere with the simultaneous injection of the particle bunches. Alternate

methods of directly coupling power into the PBG fiber using waveguide structures in the optical regime are under study [3] and may provide better efficiency for acceleration.

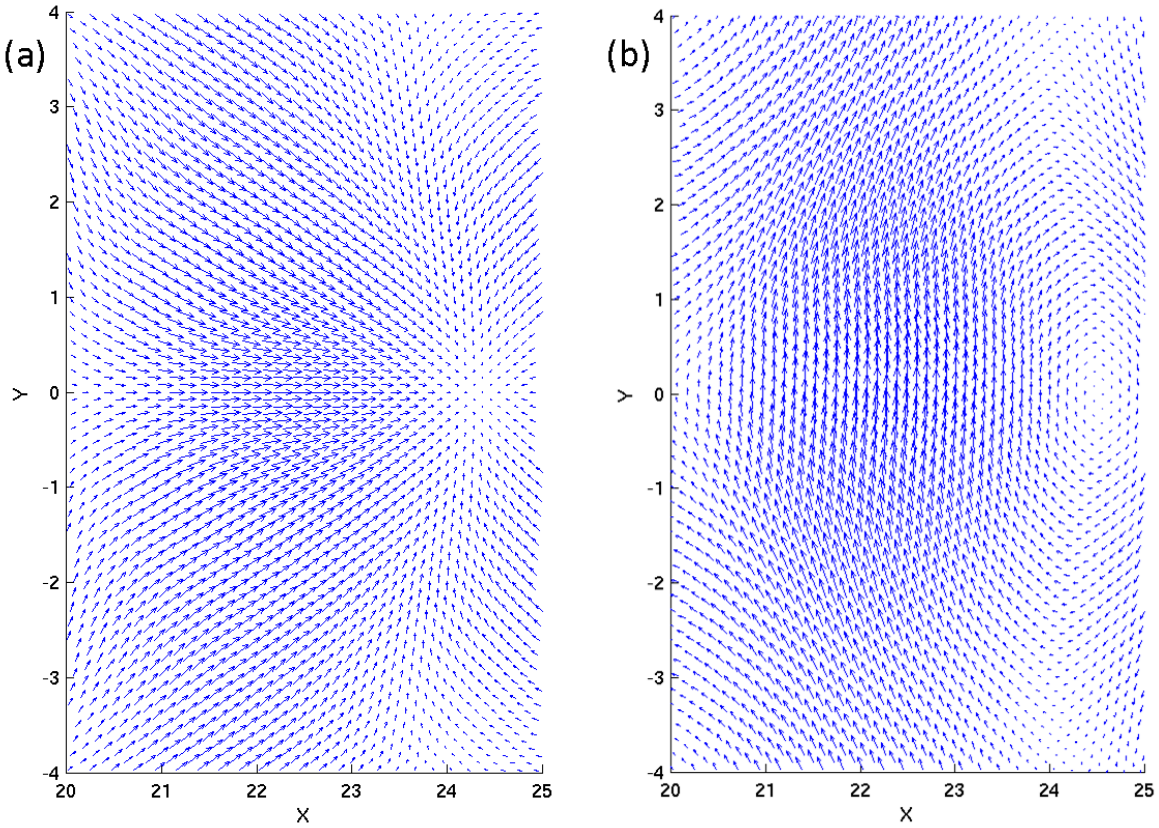

Figure 16: Polarizations of electric (a) and magnetic (b) fields in the far right hot spot ($\phi = 60^o$, $\theta = 45^o$) of the far-field radiation shown in Fig. 12 for the hemisphere radius at 80λ.

Acknowledgements

We would like to thank Eric Colby for many useful discussions and use of his Matlab code, and Greg Schussman for help with visualization. The work was supported by the U.S. DOE contract DE-AC02-76SF00515. The work used the resources of NCCS at ORNL which is supported by the Office of Science of the U.S. DOE under Contract No. DE-AC05-00OR22725, and the resource of NERSC at LBNL which is supported by the Office of Science of the U.S. DOE under Contract No. DE-AC03-76SF00098.

References

[1] X. E. Lin, Phys. Rev. ST Accel. Beams **4**, 051301 (2001).

[2] ACE3P: An Advanced Computational Electromagnetic Simulation Suite, https://confluence.slac.stanford.edu/display/AdvComp/ACE3P+-+Advanced+Computational+Electromagnetic+Simulation+Suite.

[3] R. J. England et al., *Calculation of Coupling Efficiencies for Laser-Driven Photonic Bandgap Structures*, Proc. of 2010 Advanced Accelerator Concepts Workshop.

[4] L.-Q. Lee et al., *Omega3P: A Parallel Finite-Element Eigenmode Analysis Code for Accelerator Cavities*, Tech. Report, SLAC-PUB-13529, 2009.

[5] A. E. Candel et al., *Parallel Higher-Order Finite Element Method for Accurate Field Computations in Wakefield and PIC Simulations*, Proceedings of International Computational Accelerator Physics Conference, Chamonix Mont-Blanc, France, 2006.

[6] K. Leung and Y. Liu, Phys. Rev. Lett. **65**, 2646 (1990).

[7] L. Diaz and T. Millagan, *Antenna - Engineering Using Physical Optics*, Artech House, Inc., 1996.

[8] E. Colby, private communications.

[9] B. Kuhlmey, CUDOS MoF Utilities for micro-structured optical fibres, University of Sydney, Australia. http://www.physics.usyd.edu.au/cudos/mofsoftware.